2017-24-0029

Experimental validation of combustion models for Diesel Engines based on tabulated kinetics in a wide range of operating conditions

Author, co-author list (Do NOT enter this information. It will be pulled from participant tab in MyTechZone)

Affiliation (Do NOT enter this information. It will be pulled from participant tab in MyTechZone)

Abstract

Computational fluid dynamics represents a useful tool to support the design and development of Heavy Duty Engines, making possible to test the effects of injection strategies and combustion chamber design for a wide range of operating conditions. Predictive models are required to ensure accurate estimations of heat release and the main pollutant emissions within a limited amount of time. For this reason, both detailed chemistry and turbulence chemistry interaction need to be included. In this work, the authors intend to apply combustion models based on tabulated kinetics for the prediction of Diesel combustion in Heavy Duty Engines. Four different approaches were considered: well-mixed model, presumed PDF, representative interactive flamelets and flamelet progress variable. Tabulated kinetics was also used for the estimation of NO_x emissions. The proposed numerical methodology was implemented into the Lib-ICE code, based on the OpenFOAM®technology, and validated against experimental data from a light-duty FPT engine. Ten points were considered at different loads and speeds where the engine operates under both conventional Diesel combustion and PCCI mode. A detailed comparison between computed and experimental data was performed in terms of in-cylinder pressure and NO_x emissions.

Introduction

Detailed and predictive models are necessary to support the development of new combustion systems of Diesel engines where a contemporary reduction of fuel consumption and pollutant emissions is required for a wide range of operating conditions in order to fulfill future emissions standards [1, 2]. To identify the most promising solutions, effects of combustion chamber design, injection strategy, EGR and compression ratio must be studied simultaneously and for this reason robust, accurate and fast approaches are required. In the last decade, most of the efforts were focused on incorporating detailed kinetics in Diesel spray combustion simulations with or without turbulence-chemistry interaction to predict ignition delay, flame structure (lift-off and PAH) and the main pollutant emissions [3, 4, 5, 6]. However, to accurately describe the oxidation of complex fuels including the formation of soot precursors, a large number of species and reactions is necessary with a consequent increase of computational time, since ODE stiff solvers are employed to compute the chemical reaction rates and as many transport equations as the number of involved species have to be solved. Such aspects limit the mechanism size to be used in practical simulations to approximately 100 species, despite the use of complex fuel formulations or advanced combustion modes require more species to accurately predict experimental values of laminar flame speed and ignition delay. Within this context, a possible alternative for the reduction of CPU time can be represented by tabulated kinetics: chemical species reaction rates are stored in a table according to a specified mechanism and flame structure; then they are retrieved as function of the state of the system. The most widely used approaches consider a progress variable to characterize the advancement of the fuel oxidation reactions, by solving a transport equation with a source term which depends on local thermodynamic conditions, the progress variable itself and parameters characterizing the assumed flame structure, like the mixture fraction variance or the scalar dissipation rate [7, 8, 9, 10, 11]. In a previous work [12], the authors have implemented different models for Diesel combustion into the Lib-ICE code based on tabulated kinetics, demonstrating its consistency with the approaches based on direct-integration following extensive validation against the spray-A experimental data-sets from the Engine Combustion Network.

Purpose of this work is the extension of the previously proposed approach for tabulated kinetics to include an additional combustion model as well as the possibility to predict NO_x emissions. The model presented here, called TFPV

(tabulated flamelet progress variable) was proposed in past works [10, 11, 13] and is based on the tabulation of laminar diffusion flamelets for different scalar dissipation rate levels. Compared to the multiple representative interactive flamelet model, TFPV is expected to perform better since it takes into account the local flow conditions and also transport of progress variable allow a more realistic description of the combustion process originated by multiple injections. Concerning the nitrogen oxide emissions: a transport equation is solved for a NO_x progress variable whose reaction rate is taken from auto-ignition calculations in a homogeneous reactor and this makes possible to account for both prompt and thermal formation mechanisms. The choice of using homogeneous reactors for the calculation of NO_x is justified by the fact that their formation rate is much lower compared to the other chemical species involved in the combustion process and for this reason such strong assumption can be retained.

To validate the proposed models based on tabulated kinetics, the FPT F1C Euro 6 engine was simulated under different operating conditions: eight points represent conventional Diesel combustion, while the capability to predict PCCI mode was also evaluated in a different version of the considered engine with reduced compression ratio. Calculations were carried out with the Lib-ICE code, based on the OpenFOAM®technology, using four different combustion models based on tabulated kinetics: well-mixed (TWM), presumed PDF (TPPDF), tabulated representative interactive flamelet (TRIF) and flamelet progress variable (FPV). Validation was carried out by comparing computed and experimental data of in-cylinder pressure, apparent heat release rate and nitrogen oxide emissions.

Combustion Models

Tabulated kinetics is incorporated into four different combustion models: well-mixed (TWM), presumed PDF (TPPDF), representative interactive flamelets (TRIF) and flamelet progress variable (TFPV). TWM, TPPDF and TRIF are extensively described and validated under constant-volume combustion conditions in [12].

Chemistry table generation

Fig. 1 reports the way chemistry is tabulated in the proposed approach. The user specifies a chemical mechanisms and a range of initial conditions for homogeneous, constant-pressure reactor calculations in terms of mixture fraction Z, ambient pressure p, initial reactor temperature T_u and residual gas fraction. Initial reactor composition is computed from this information and simulations of constant-pressure, auto-ignition process are performed to generate the chemistry table. In spray combustion problems, the user well knows the values of the oxidizer temperature $T(Z=0)$, the one of the liquid fuel $T(Z=1)$ and the fuel heat of evaporation, hence it is more convenient to express the initial reactor temperature as function of such quantities for a better description of the expected states of the system:

$$h(Z) = (1-Z)\cdot h(T_{Z=0}) + Z\cdot h(T_{Z=1}) - Z\cdot h_l(T_{Z=1}) \quad (1)$$

$$T_u(Z) = T(h(Z)) \quad (2)$$

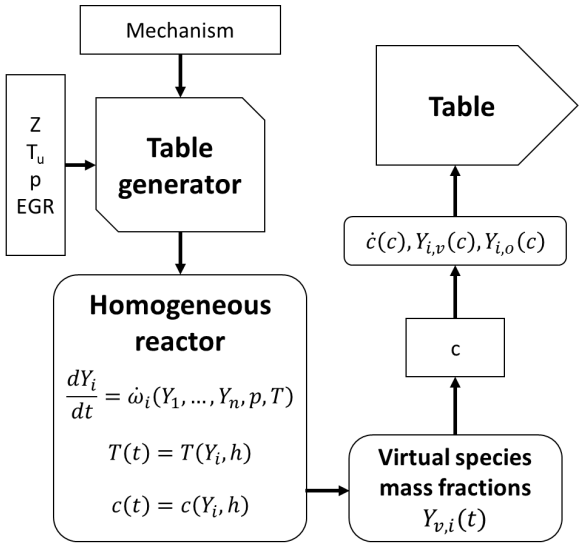

Figure 1: Generation of the chemistry table based on the homogeneous reactor assumption.

Homogeneous reactor, auto-ignition calculations at constant pressure are performed by solving chemical species equation:

$$\frac{dY_i}{dt} = \dot{\omega}_i\left(T, p, Y_1, ..., Y_n\right) \quad (3)$$

with reactor temperature T computed directly from the initial enthalpy value. After every time-step, the progress variable C is evaluated and the equivalent reactor chemical composition is computed by means of the *virtual species approach* [14, 12]. Progress variable is defined as in [13], with C being equal to the heat released by combustion, computed as the difference between the current and the initial value of the reactor formation enthalpy, also known as h_{298}:

$$C = \sum_{i=1}^{Ns} h_{298,i} \cdot Y_i\left(t\right) - \sum_{i=1}^{Ns} h_{298,i} \cdot Y_i\left(0\right) \quad (4)$$

where N_s is the total number of chemical species used by the specified mechanism. The adopted definition for C uniquely characterizes each point in the thermochemical state space and is appropriate for a transport equation. At the end of each reactor calculation, progress variable reaction rates and chemical composition are stored as function of the discrete values of the normalized progress variable c, specified by the user:

$$c = \frac{C - C_{min}}{C_{max} - C_{min}} \quad (5)$$

where C_{min} and C_{max} are minimum and maximum values of the progress variable which are found at initial and after auto-ignition conditions. C_{min} and C_{max} are stored in the table as function of Z,T_u,p. From the values of times at which the specified c_i values were found, the progress variable reaction rate is computed with the forward differencing scheme as follows:

$$\dot{c}_i = \frac{c_{i+1} - c_i}{t_{i+1} - t_i} \tag{6}$$

$\dot{c}$ is then multiplied by the term $C_{max} - C_{min}$ in order to have the proper source term $\dot{C}$ in the progress variable transport equation. For any tabulated value of the progress variable c, the chemical composition is also stored. To avoid the storage of the entire set of species and keep an acceptable size of the table, only seven ones named *virtual* species are tabulated and their mass fractions are computed in order to preserve the main thermochemical properties of the full set used in the detailed mechanism. Virtual species used in this work are N_2, O_2, $fuel$, CO_2, CO, H_2O, H_2 and their composition is computed for any c in order to conserve the main properties of the full set of species:

1. total number of C, H, N and O atoms
2. mixture enthalpy and specific heat
3. mixture molecular mass

Constant-volume and constant pressure reactor calculations performed in a wide range of conditions made possible to verify that cumulative heat release, reactor temperature and pressure evolutions are consistent with the cases where the full set of species is used. The table also includes the mass fractions of chemical species which are of interest for the user (Y_o in Fig. 1), either for post-processing reason or because they are relevant for the formation of the main pollutants and have to be used by the related sub-models.

Governing equations

In the CFD domain, transport equations for mixture fraction, enthalpy, unburned gas temperature and progress variable are solved and then the table is accessed with the local cell values to compute the progress variable reaction rate and the chemical composition. Interpolation of table values at cell conditions is performed by means of an inverse, distance weighted technique. The progress variable source term used in the C transport equation depends on which combustion model is used:

$$\frac{\partial \bar{\rho}\tilde{C}}{\partial t} + \nabla(\bar{\rho}\tilde{\mathbf{U}}\tilde{C}) - \nabla\left(\frac{\tilde{\mu}_t}{Sc_t}\nabla\tilde{C}\right) = \rho\dot{C} \tag{7}$$

To consistently access the table data, it is necessary to solve an additional equation for the unburned gas enthalpy which is then used to estimate the unburned gas temperature T_u which is one of the independent variables of the table:

$$\frac{\partial \bar{\rho}\tilde{h}_u}{\partial t} + \nabla(\bar{\rho}\tilde{\mathbf{U}}\tilde{h}_u) - \nabla\left(\tilde{\alpha}_t\nabla\tilde{h}_u\right) = \dot{Q}_s + \frac{\bar{\rho}}{\bar{\rho}_u}\cdot\frac{D\bar{p}}{Dt} \tag{8}$$

where α_t is the turbulent thermal diffusivity and ρ_u is the density of unburned gases which is computed from cell pressure, chemical composition at $C = 0$ and T_u. $\dot{Q}_s$ is the term related to spray evaporation which assumes different values in case the mixing line is assumed or not in the table generation process.

Tabulated well mixed model (TWM)

Tabulated well-mixed model does not include any interaction between turbulence and chemistry and for this reason, the progress variable source term to be used in Eq. 7 is directly taken from Eq. 6:

$$\dot{C} = (C_{max} - C_{min}) \cdot \dot{c} \tag{9}$$

The operation of the tabulated well-mixed model is reported in Fig. 2 and the user is referred to [12] for further details. To ensure a consistency between TWM and the corresponding approach based on direct integration, avoiding anticipated ignition due to progress variable diffusion from rich to lean side after the cool flame, reaction rates are set to zero in regions where dual-stage ignition does not happen, corresponding approximately to an equivalence ratio value $\phi = 3$.

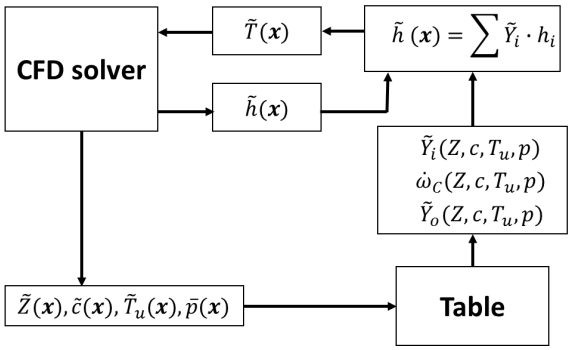

Figure 2: Operation of the tabulated well-mixed combustion model (TWM).

Tabulated presumed PDF combustion model (TPPDF)

This approach includes turbulence/chemistry interaction and it was applied in [15, 16] to simulation of compression-ignition engines. Progress variable source term is computed assuming a δ-PDF distribution for the progress variable and a β-PDF function was used for the mixture fraction:

$$\dot{C} = \int_0^1 \int_0^1 \dot{C}\,(p, T_u, Z, c)\,\beta\left(Z, \widetilde{Z''^2}\right)\delta\,(c)\,dc\,dZ \tag{10}$$

Computation of $\beta\left(Z,\widetilde{Z''^2}\right)$ requires to additionally solve the mixture fraction variance $\widetilde{Z''^2}$ equation:

$$\frac{\partial\bar{\rho}\widetilde{Z''^2}}{\partial t}+\nabla(\bar{\rho}\tilde{\mathbf{U}}\widetilde{Z''^2})-\nabla\left(\tilde{\mu}_t\nabla\widetilde{Z''^2}\right)=2\frac{\tilde{\mu}_t}{Sc}\left|\nabla\tilde{Z}\right|^2-\bar{\rho}\tilde{\chi} \tag{11}$$

The sink term appearing in Eq. 11 is the average scalar dissipation rate, which is function of the turbulent time scale and mixture fraction variance:

$$\tilde{\chi}=C_\chi\frac{\tilde{\varepsilon}}{\tilde{k}}\widetilde{Z''^2} \tag{12}$$

The TPPDF table is generated by processing the homogeneous reactor table to include the effects of turbulence chemistry interaction, as shown in Fig. 3. In particular, the user specifies a range of mixture fraction segregation factors S_Z, defined as the ratio between $\widetilde{Z''^2}$ and the maximum variance values:

$$S_Z=\frac{\widetilde{Z''^2}}{\tilde{Z}(1-\tilde{Z})} \tag{13}$$

for any value of Z and S_Z it is possible to compute variances and the coefficients for the probability density function distributions. On the basis of them, integration is performed for all the tabulated quantities f_{HR} following Eq. 10 and a new table including the effects of mixture fraction fluctuations is available for the presumed PDF combustion model. Turbulence/chemistry interaction in the TPPDF model considers only the effects of local fluctuations of Z, but it does not consider any sub-grid diffusion in the mixture fraction space, as it is commonly done in transported PDF or laminar flamelet models [17, 18]. Table processing in order to perform the β-PDF integration in the mixture fraction space requires approximately an additional 20% of the time which is needed for the generation of the homogeneous reactor table.

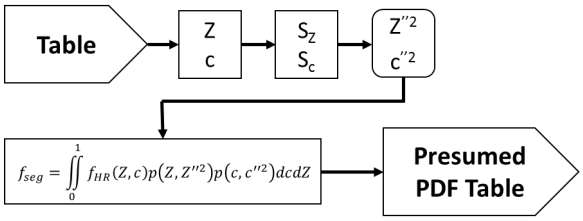

Figure 3: Generation of the chemistry table used for the presumed PDF combustion model (TPPDF).

Tabulated representative interactive flamelet model (TRIF)

This model is based on the laminar flamelet concept, assuming that there exists a locally undisturbed sheet where reactions occur [5]. This sheet can be treated as an ensemble of stretched counter-flow diffusion flames, called *flamelets*. In this way, all reacting scalars only depend on the mixture fraction variable, Z, which is related to the local fuel-to-air ratio for non-premixed combustion. Hence, local chemical composition can be estimated from the Z field in the CFD domain, assuming that its sub-grid distribution can be represented by a β-PDF. To account for local flow and turbulence effects on the flame structure and predict flame stabilization, a multiple number of flamelets can be used. Each one is representative of a certain portion of the injected fuel mass, and chemical composition in each cell is computed from mixture fraction and flamelet marker distribution as follows:

$$\tilde{Y}_i\left(\vec{x}\right)=\sum_{j=1}^{N_f}M_j\int_0^1 Y_{j,i}\left(\tilde{Z}\right)P\left(\tilde{Z},\widetilde{Z''^2}\right)dZ \tag{14}$$

For each flamelet marker M_j, a transport equation is solved including spray evaporation source term only for a specified interval of the injection duration [3]. The local flame structure is defined by the flamelet equations that are solved for the progress variable C and enthalpy assuming unity Lewis number [5] in the mixture fraction space:

$$\rho\frac{\partial C}{\partial t}=\rho\frac{\chi_z}{2}\frac{\partial^2 C}{\partial Z^2}+\dot{C} \tag{15}$$

$$\rho\frac{\partial h}{\partial t}=\rho\frac{\chi_z}{2}\frac{\partial^2 h}{\partial Z^2}+\frac{dp}{dt} \tag{16}$$

The chemical composition in the mixture fraction space is retrieved from the chemistry table in the same way as done for the TWM model in the CFD domain. Effects of mixing related to turbulence and flow-field are grouped into the scalar dissipation rate term χ_z which is function of the scalar dissipation rate at stoichiometric mixture fraction conditions $\widetilde{\chi_{st,j}}$ which is computed for each flamelet.

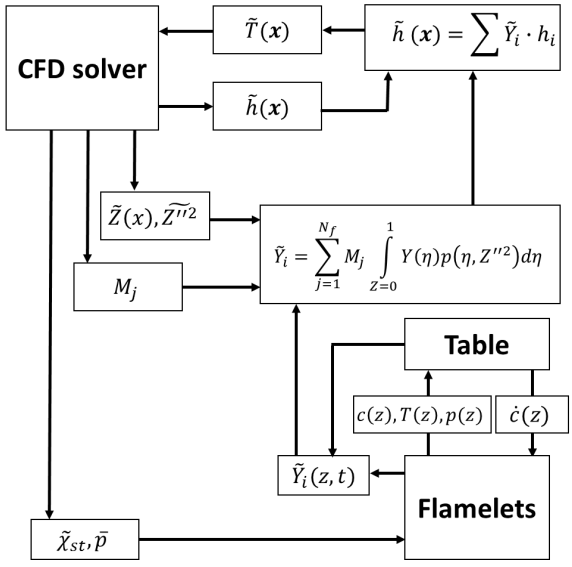

Figure 4: Operation of the tabulated representative interactive flamelet combustion model (TRIF).

The Fig. 4 summarizes the operation of the TRIF combustion model, illustrating the mutual interactions between

the CFD, flamelets domains and chemistry table. Further details about the RIF model implementation in Lib-ICE can be found in [3, 19, 20]. Despite using tabulated reaction rates, TRIF simulations will have higher computational costs compared to TWM or TPPDF due to the need to perform on-line the integration of Eq. 14 in any computational cell for any flamelet [3].

Tabulated flamelet progress variable (TFPV)

Purpose of the TFPV model is to provide a realistic description of the turbulent diffusion flame, taking into account turbulence/chemistry interaction, sub-grid mixing and premixed flame propagation. This requires to solve a transport equation for the progress variable in the CFD domain where the source term depends on local thermodynamic conditions (T, p), mixture fraction Z, mixture fraction variance $\widetilde{Z''^2}$ and stoichiometric scalar dissipation rate χ_{st}. In this way, the model is expected to give correct predictions of:

- extinction in the near nozzle region where the scalar dissipation rate is very high;
- re-ignition due to the progress variable convection and diffusion;
- flame stabilization process including effects of both premixed and diffusive flame propagation.

The TFPV library is based on unsteady diffusion flame calculations performed with the TRIF model, in a similar way as done in [13, 10, 11] with the so-called *approximated diffusion flames* approach. Generation of the TFPV library is shown in Fig. 5: the user specifies a range of temperature, pressure, and scalar dissipation values for which unsteady, diffusion flame calculations are performed using the TRIF model. At any time step, for the prescribed values of Z it is possible to estimate the chemical composition in terms of virtual species ($Y_{i,v}\left(Z,t\right)$) and the progress variable $C\left(Z,t\right)$. TRIF data are then processed at each time step to account for mixture fraction variance. For the specified values of the mixture fraction segregation S_Z, the corresponding variance value is computed, progress variable and chemical composition are estimated as follows:

$$Y_i\left(Z,\widetilde{Z''^2}\right) = \int_0^1 Y_{TRIF}\left(Z\right)\beta\left(Z,\widetilde{Z''^2}\right)dZ \qquad (17)$$

$$C\left(Z,\widetilde{Z''^2}\right) = \int_0^1 C_{TRIF}\left(Z\right)\beta\left(Z,\widetilde{Z''^2}\right)dZ \qquad (18)$$

At the end of any diffusion flame calculation, for any value of Z ad $\widetilde{Z''^2}$ the progress variable is normalized and its reaction rate is estimated following the approach described in Eqns. 5-6. Computed data are then interpolated for the specified progress variable values and then the table is generated.

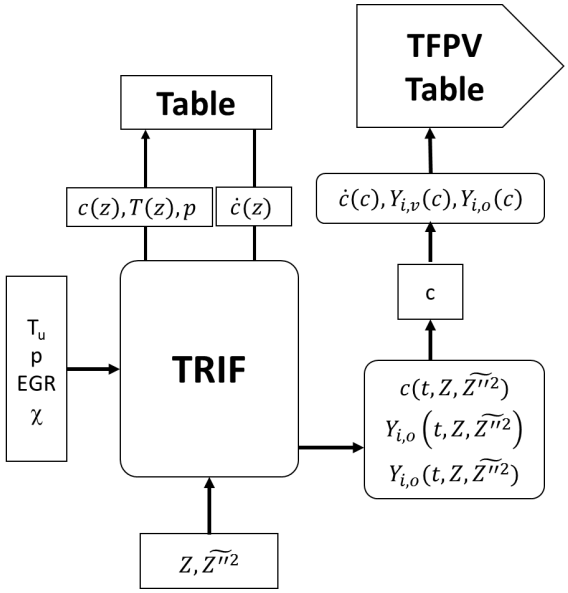

Figure 5: Generation of the Tabulated Flamelet Progress Variable (TFPV) table using the TRIF model.

To generate the TFPV table, it is necessary to run unsteady flamelet calculations for all the specified range of pressure, temperature and specified stoichiometric scalar dissipation rate values. Despite only two flamelet equations are solved within the TRIF model, the use of fixed time step (which has to be small in order to correctly account for combined effects of mixing and reaction) and need to account for different scalar dissipation rate values increases the computational time of a 5-10 factor compared to the one needed to generate the homogeneous reactor table. In the TFPV model, effects of table discretization are expected to influence the computed results in two ways:

- Chosen intervals of pressure, temperature, mixture fraction and progress variable influence results of any TRIF simulation and, in particular, the computed ignition delay;
- CFD simulation results will also depend on the scalar dissipation rate values which will be used to generate the TFPV table.

In particular, the selected range of scalar dissipation rates should be large enough to include extinction, allowing a correct description of the diffusion flame stabilization process.

NO_x emissions

A tabulated approach for the prediction of NO_x emissions was also developed to estimate their concentration as result of both prompt and thermal formation mechanisms. Suitable reactions describing the NO_x kinetics should be included. Homogeneous reactor calculations are performed until the NO_x specie, defined as:

$$Y_{NO_x} = Y_{NO} + Y_{NO_2} + Y_{N_2O} + Y_{N_2O_2} \qquad (19)$$

reaches the equilibrium value. This happens much later than the ignition, since the time-scales of NO_x formation are higher than the ones governing the fuel oxidation: this aspect is shown, in terms of normalized values, in Fig. 6. Hence, formation rate of NO_x cannot be expressed only as function of the main thermodynamic conditions and progress variable as it is done for the composition and the progress variable reaction rate.

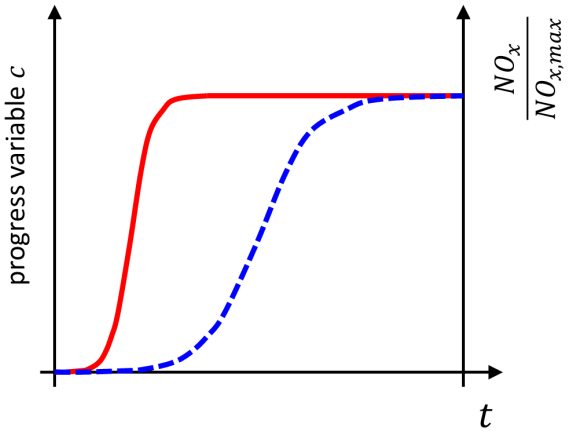

Figure 6: Evolution of normalized progress variable and normalized NO_x as function of time for an auto-ignition event in a constant-pressure reactor.

A transport equation is solved for the Y_{NO_x} as follows:

$$\frac{\partial \bar{\rho}\tilde{Y}_{NO_x}}{\partial t} + \nabla \cdot \left(\bar{\rho}\tilde{\mathbf{U}}\tilde{Y}_{NO_x}\right) - \nabla \cdot \left(\frac{\tilde{\mu}_t}{Sc_t}\nabla \tilde{Y}_{NO_x}\right) = \dot{\omega}_{NO_x} \tag{20}$$

$\dot{\omega}_{NO_x}$ should account for both NO_x formation during the ignition process (*prompt*) and afterwards (*thermal*). This is done by processing homogeneous reactor calculations. At any time-step, the current value of Y_{NO_x} is evaluated according to Eq. 19 and, at the end of any reactor calculation, the maximum NO_x value Y_{eq,NO_x} is evaluated and stored in the table as function of the initial thermodynamic conditions (p, T_u, Z, EGR). From user-specified values of the NO_x progress variable c_{NO_x}, defined as:

$$c_{NO_x} = \frac{Y_{NO_x}}{Y_{eq,NO_x}} \tag{21}$$

the normalized reaction rate $\dot{c}_{NO_x}$ is evaluated as function:

1. of the normalized combustion progress variable c:

$$\dot{c}_{NO_x,1} = \frac{c_{NO_x}\left(c_{i+1}\right) - c_{NO_x}\left(c_i\right)}{t\left(c_{i+1}\right) - t\left(c_i\right)} \tag{22}$$

   where $c_{NO_x,i}$ is the value of the NO_x progress variable corresponding to the normalized progress variable c_i found at time t_i;

2. of the normalized NO_x progress variable c_{NO_x}:

$$\dot{c}_{NO_x,2} = \frac{c_{NO_x,i+1} - c_{NO_x,i}}{t\left(c_{NO_x,i+1}\right) - t\left(c_{NO_x,i}\right)} \tag{23}$$

The source term of Eq. 20, $\dot{\omega}_{NO_x}$, is then computed as:

$$\dot{\omega}_{NO_x} = \rho Y_{eq,NO_x}\dot{c}_{NO_x,1} \quad if \quad c < \bar{c} \tag{24}$$

$$\dot{\omega}_{NO_x} = \rho Y_{eq,NO_x}\dot{c}_{NO_x,2} \quad if \quad c \geq \bar{c} \tag{25}$$

where $\bar{c}$ is a threshold value which is set to 0.99. The sensitivity of the computed NO_x values from $\bar{c}$ is low, provided that a sufficiently high value is selected ($\bar{c} > 0.5$). The proposed approach makes possible to consistently distinguish between prompt and thermal NO_x formation.

Spray and turbulence modeling

The Eulerian-Lagrangian approach is used to model the spray evolution where the spray is described by a discrete number of computational *parcels*, each one representing droplets with the same properties. The spray parcels evolve into the computational domain according to the mass, momentum and energy exchange with the continuous gas phase which is treated in an Eulerian way. Specific sub-models are necessary to describe fuel atomization, breakup, heat transfer, evaporation, collision and wall impingement. In this work, parcels are introduced in the CFD domain with the same nozzle diameter, their initial velocity depends on injected mass flow rate profile and the spray angle is function of nozzle geometry and liquid to gas density ratio [21]. Jet and droplet breakup are computed by the KHRT model, which accounts for both Kelvin-Helmholtz (KH) and Rayleigh-Taylor (RT) instabilities [22]. To avoid unphysical formation of too small droplets in the vicinity of the nozzle, RT breakup is possible only at a certain distance from it. Such distance is known as *breakup length* and is function of nozzle diameter and liquid to gas density ratio. Concerning other sub-models used, droplet evaporation is computed on the basis of the D^2 law and the Spalding mass number while the Ranz-Marshall correlation was used to model heat transfer between liquid and gas phases. Collision is neglected since it plays a minor role in evaporating sprays [23].

The standard $k - \varepsilon$ model was used for turbulence with the C_1 constant modified to 1.5 as it is commonly done to predict penetration and diffusion of jets. Validation of the proposed methodology for spray modeling at non reacting conditions is illustrated in [24, 20] where a detailed comparison between computed and experimental data is reported for spray penetration and radial distribution of mixture fraction.

Mesh management

ECN Spray A simulations were carried out in a 2D axysymmetric graded mesh, with an average cell size of 0.5 mm and progressively refined close to the nozzle, where the minimum size is approximately 2 mm. For the simulation of compression, combustion and the expansion phases in a

Diesel engine, the mesh handling technique developed by the authors over the years makes possible to emply only a single grid whose topology is changed during the motion of the piston [25, 26]. During the mesh generation stage, the user identifies a inner set of cell faces where layers of cells are added or removed, given the corresponding minimum and maximum cell thicknesses. As points move, cell layers in front of the interface change and layer addition or removal is triggered with no user action. The proposed technique supports hexahedral cells and there are no limitations on the flatness of the oriented base surface. This improves the flexibility of the approach mainly in case of Diesel engine simulations, making possible to keep the mesh orientation to the spray in the injector region during piston motion as shown in Fig. 7.

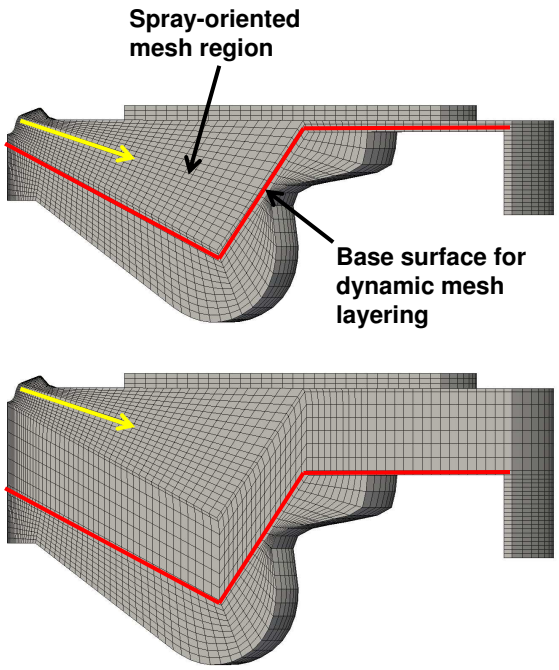

Figure 7: Operation of dynamic mesh layering in a spray-oriented grid. Line in red: base oriented set of faces (user defined); yellow line: injection direction. (a) Mesh at TDC; (b) Mesh at 20 CAD after TDC.

Experimental Validation

Experiments carried out in a constant-volume vessel with n-dodecane (Spray A) and a light-duty Diesel engine were used to assess and validate the proposed combustion models based on tabulated kinetics. Diesel fuel was assumed to be $n - C_{12}H_{26}$ and in this work its oxidation was modeled using the mechanism proposed by Frassoldati et al. [27]. It has 96 species and 993 reactions and it was extensively validated with experimental data in a wide range of conditions including flow and stirred reactor experiments, auto-ignition delay times, laminar flame speeds, and auto-ignition of isolated fuel droplets in micro-gravity conditions.

Validation of the TFPV Model

A preliminary assessment and validation of the TFPV model was performed in a similar way as done for the other approaches in [12]. In particular, the well-known constant-volume spray-A experiment from ECN [28, 29, 30] was simulated at different ambient conditions including variations of ambient temperature and ambient oxygen concentration. The setup used for the table is reported in Tab. 1. The chosen values of the stoichiometic scalar dissipation rate follows a log-law. Discretization of the TFPV table chosen in this work was mainly a compromise between accuracy, required computational time to generate one table and memory needed to store the data.

Table 1: Chemistry table discretization used for the simulation of the spray-A experiment.

Temperature [K]	700-1000 (step 20 K) 1000-1100 (step 25 K) 1100-1200 (step 50 K)
Equivalence ratio	0, 0.2, 0.4, 0.5, 0.6, 0.7-1.4 (step 0.05), 1.5-2 (step 0.1), 2-3 (step 0.2)
Pressure [bar]	40, 45, 50, 55 60, 70, 80
Mixture fraction segregation	0, 0.005, 0.01, 0.05, 0.1, 1
Scalar dissipation rate χ_{st} [1/s]	0, 1, 3, 7, 20, 55

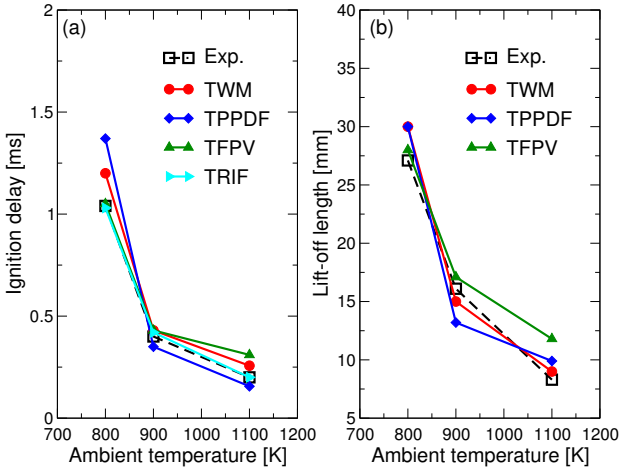

Figure 8: Comparison between experimental data and computed ones from TWM, TPPDF, TRIF and TFPV models as function of ambient temperature: (a) Ignition delay; (b) Flame-lift off.

Figs. 8 and 9 reports comparison between computed and experimental values of ignition delay and flame lift-off. For the TRIF model, lift-off length is not reported since only one flamelet was used [12] and in such case the flame is anchored to the nozzle. In a future work, simulations will be carried out with TRIF and multiple flamelets in order to properly estimate the flame lift-off when such model is used. As expected, TFPV and TRIF have a similar agree-

ment in terms of ignition delay except for the slight overestimation at 1100 K ambient temperature. Dependency on the ambient oxygen concentration is correctly captured either for both ignition delay and flame lift-off. All the models overpredict ignition delay when oxygen concentration is low and this aspect is mainly related to the used kinetic mechanism, as illustrated in detail in [27].

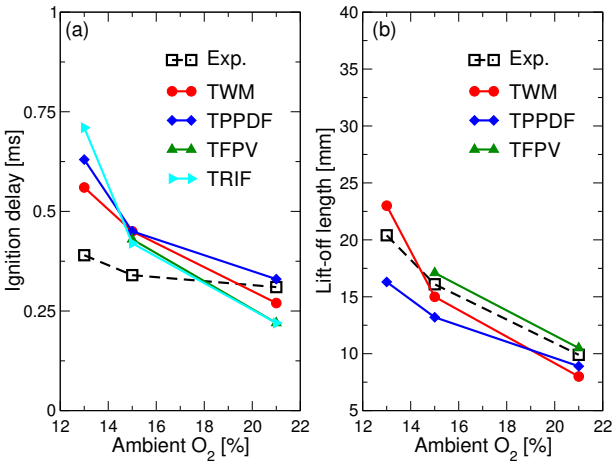

Figure 9: Comparison between experimental data and computed ones from TWM, TPPDF, TRIF and TFPV models as function of ambient oxygen concentration: (a) Ignition delay; (b) Flame-lift off.

To understand how sub-grid mixing affects heat release rate (HRR), a comparison between experimental and computed vessel pressure rates is illustrated in Fig. 10 for the *baseline* conditions with 900 K ambient temperature, 22.8 kg/m^3 ambient density, 15% of ambient oxygen concentration and 1500 bar of injection pressure. The TPPDF, TRIF and TFPV combustion models were chosen for this comparison since all of them account for turbulence chemistry interaction despite in different ways. The models have different behaviors mainly before the ignition delay time: in TRIF and TFPV, ignition is a two-stage process and the time interval between the two events, known as *thermal runaway*, can be clearly distinguished. That period is characterized by a substantial balancing between reaction and diffusion [5]. The TPPDF predicts a single-stage ignition process instead. This is mainly related to the way the progress variable source term is computed: Eq. 10 accounts for mixture fraction fluctuations, but performs the integration assuming the same progress variable value in the whole Z-domain. This assumption is in contrast with what is normally happening in diffusion flame auto-ignition, where the progress of combustion is not uniform in the mixture fraction space and is governed by diffusion and chemistry simultaneously [31].

Finally, in Fig. 11 a comparison between computed temperature distributions by TPPDF and TFPV models is also reported for the baseline condition together with the isocontour of stoichiometric mixture fraction and the experimental location of the lift-off length. Two stage ignition and effects of scalar dissipation rate are the reason why in TFPV model the flame stabilizes at a longer distance from the nozzle with a better agreement with experimental data. TPPDF and TFPV have very similar maximum temperature values and temperature distributions far from the lift-off length, and this is the main reason of similar HRR predictions.

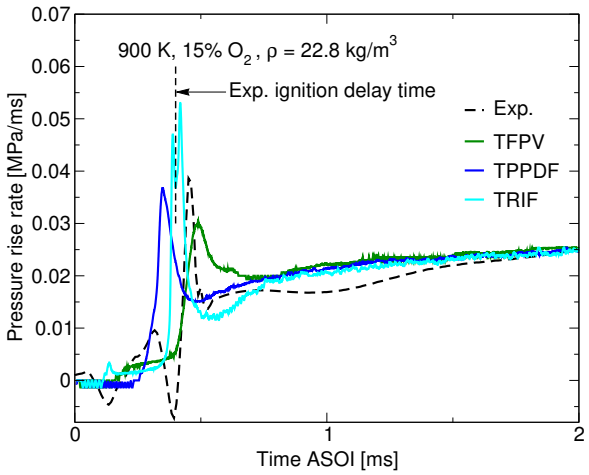

Figure 10: Comparison between experimental vessel pressure rise rate the ones computed by TPPDF, TRIF and TFPV combustion models.

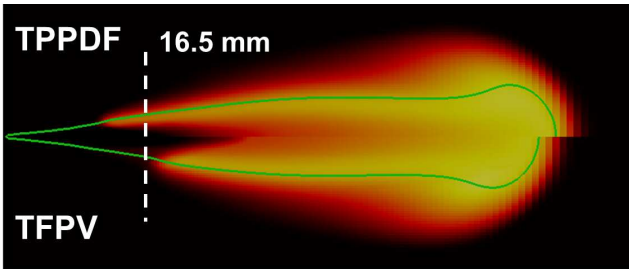

Figure 11: Computed temperature distribution for the TWM and TPPDF models. Temperature range: 900 (black) - 2300 (yellow).

In [12], the authors have illustrated the consistency between direct integration and tabulated kinetics for both the TRIF and TWM models. Such comparison cannot be easily done for the TFPV model, since there is not a corresponding model where chemistry can be directly integrated. A possible candidate could be a multi-RIF model where interaction between different flamelets is taken into account to mimick the diffusion of the progress variable in absence of mixture fraction gradient. This comparison will be matter of investigation in a future work.

FPT F1C Engine

The FPT F1C light-duty Diesel engine was simulated under different operating conditions to validate the proposed combustion models. Details of the piston bowl geometry are provided in Fig. 13(b) together with the main engine

data reported in Tab. 2. Conventional Diesel combustion was first considered and simulations were carried out for eight different operating which are of interest for the engine operation shown in Fig. 12. Details of the simulated conditions are illustrated in Tab. 3, where it is possible to see that conditions with different injections, loads and level of EGR were investigated.

Table 2: Main geometry data of the FPT F1C engine simulated in this work.

Bore	96 mm
Stroke	104 mm
Compression ratio	18
IVC	-145 deg
EVO	110 deg
Swirl ratio	1.3
Number of injector holes	8
Nozzle hole diameter	140 μm

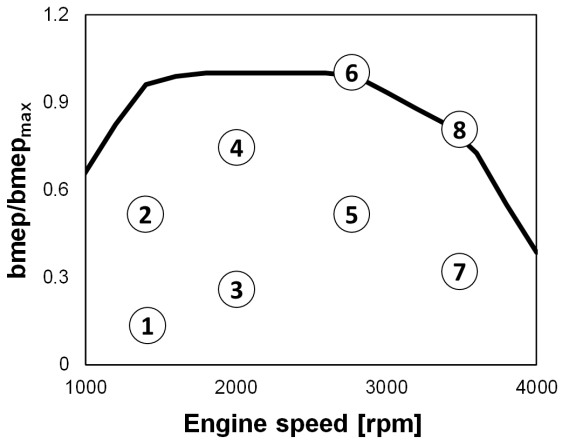

Figure 12: Operating map of the F1C engine and simulated operating points.

Table 3: Simulated operating points for the F1C engine under conventional Diesel Combustion mode.

	Name	speed [rpm]	load	λ	EGR	#inj
1	HEGR	1400	12%	2.7	40%	3
2	1400x50	1400	50%	1.4	15%	3
3	A25	2000	25%	2.1	20%	3
4	A75	2000	75%	1.3	15%	3
5	B50	2750	50%	1.4	15%	3
6	B100	2750	100%	1.3	5%	2
7	C40	3500	40%	2.3	10%	3
8	C100	3500	100%	1.5	0%	1

Calculations were run with eight different chemistry tables, one for each operating point, with the oxidizer chemical composition estimated by an extensively validated 1D model of the whole engine system. The table discretization used for all the Diesel engine combustion simulations is reported in Tab. 4 and was determined after a preliminary sensitivity analysis using the tabulated well-mixed model for what concerns the selected temperature, pressure and mixture fraction intervals. Any further refinement of such quantities does not improve the predicted ignition delays and heat release rate profiles. The selected temperature and pressure ranges take into account all the expected thermodynamic states of the system encountered during the engine simulations. The time required to generate the homogeneous reactor chemistry table is about one hour on eight cores and six hours were needed to generate the TFPV table. Any engine simulation from IVC to EVO is completed in approximately 18 hours on the same number of cores (each node is dual-core, eight processor Intel Xeon E5-2630 v3 2.40GHz).

Table 4: Chemistry table discretization used for the simulation of the FPT F1C engine

Temperature [K]	600, 650, 700, 750, 800, 850, 900, 950, 1000 1100 1200 1300
Pressure [bar]	30 70 110 150 200
Equivalence ratio	0, 0.4, 0.5, 0.6, 0.7, 0.75, 0.8, 0.85, 0.9, 0.95, 1, 1.05, 1.1, 1.15, 1.2, 1.25, 1.3, 1.35, 1.4, 1.5, 1.6, 1.7, 1.8, 1.9, 2, 3
Mixture fraction segregation	0.0 0.001 0.0025 0.01, 0.025 0.1 1.0
Scalar dissipation rate χ_{st} [1/s]	0, 1, 3, 7, 20, 55

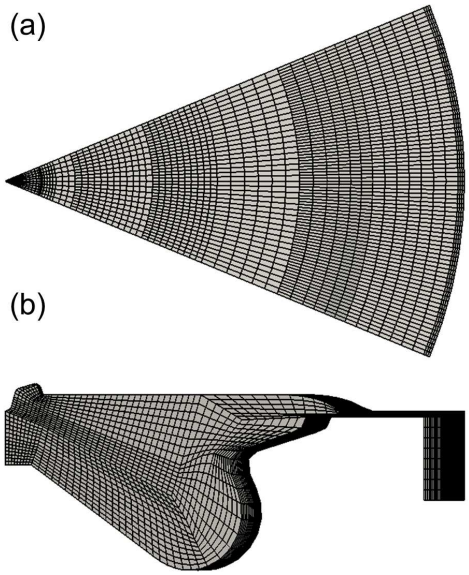

Figure 13: Computational mesh of the F1C engine: (a) Top view; (b) side view.

The spray-oriented grid of the F1C engine was automatically generated using the algorithms presented in [32] and mesh details are provided in Fig. 13. Simulations start at IVC imposing a wheel-flow velocity profile whose intensity is proportional to the swirl number which was measured at the flow bench under steady-state flow conditions. The mesh has 250000 cells at IVC which are reduced to

40000 at TDC because during mesh motion the dynamic layering technique was employed [32]. The mesh resolution in the tangential direction is continuously increased to keep an optimum mesh size which is necessary to predict fuel-air mixing and temperature distribution during the combustion process.

For a detailed validation analysis, four different points were considered, with different speeds and loads: C100, B50, A25 and HEGR. Fig. 14 compares experimental data of in-cylinder pressure and apparent rate of heat release (AHRR) for the C100 condition, representing full load operation at the highest considered speed. At this operating condition, the performance of the three tested models in terms of cylinder pressure and heat release rate is rather similar. TRIF has the highest pressure peak, mainly because it ignites earlier than TPPDF and TFPV. All models underpredict significantly the AHRR trace 10 degrees after the Top Dead Center (TDC) and possible reasons for such behavior could be found in the used mesh structure and size, turbulence model and the uncertainties related to the injected mass flow rate profile used under such condition.

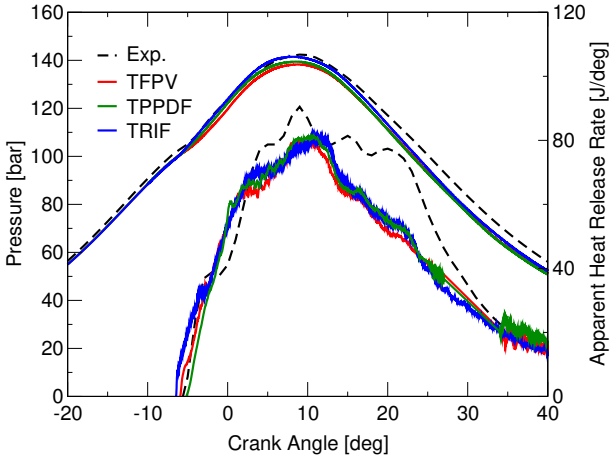

Figure 14: Comparison between computed and experimental data of in-cylinder pressure and apparent heat release rate for the operating point C100.

When reducing the load and speed and introducing pilot injections, the effects of the combustion model become more relevant. Fig. 15 reports the results for the B50 case: the AHRR profile clearly shows the presence of three different peaks corresponding to the three separated injection events. All the three models predicts correctly the in-cylinder pressure evolution with TRIF and TFPV profiles being very similar and smoother than TPPDF in the ramp of the AHRR which follows the main injection. To better understand the differences between the involved combustion models, Fig. 16 reports the AHRR profiles resulting from the two injection events more in detail. The TRIF model employs three different flamelets in this case (one for any injection) and is characterized by two intense peaks of heat release following the two pilot injections: the reason for such behavior can be related to two aspects: first, the use of a single value of the scalar dissipation rate to characterize the whole amount of mixture fraction originating from a single injection event. Furthermore, since there is no interaction between the different flamelets, ignition delay from the second pilot and the main injection events are slightly overestimated. The TFPV model accounts for local distribution of the scalar dissipation, and this is probably the reason for a smoothed AHRR peak after the first ignition. Convection and diffusion of progress variable makes the predicted ignition delay of the second pilot injection closer to the experimental one. Lack of sub-grid mixing in the TPPDF model is responsible for lower AHRR peaks.

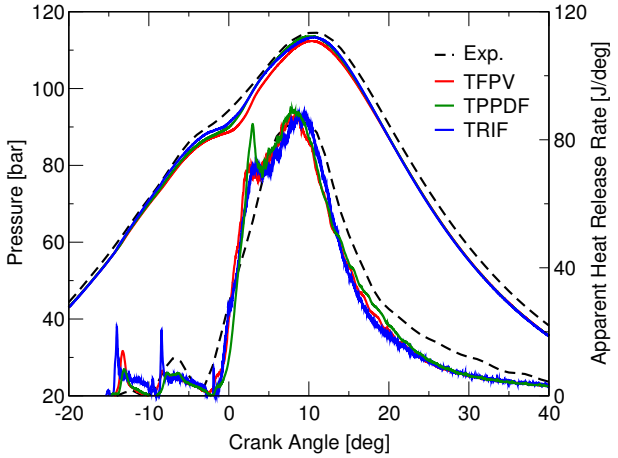

Figure 15: Comparison between computed and experimental data of in-cylinder pressure and apparent heat release rate for the operating point B50.

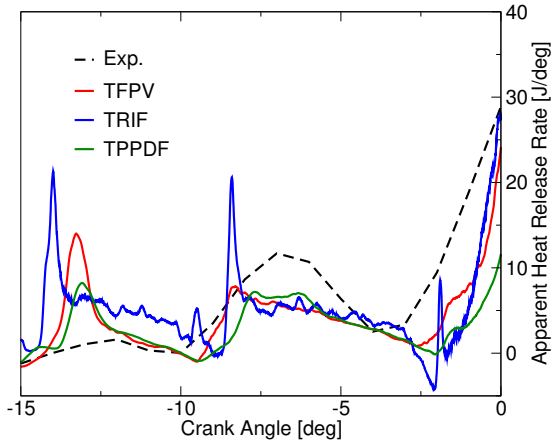

Figure 16: Comparison between computed and experimental data of in-cylinder pressure and apparent heat release rate for the operating point B50 during the pilot injection events.

Further reduction of load and speed with increase of EGR in A25 (Fig. 17) and HEGR (Fig. 18) conditions gives even more importance to the effects of pilot injections on the combustion process. For both these conditions, results are in rather good agreement with experimental data for the

three models, with the TFPV model having the best agreement in terms of AHHR but a slight underestimation of cylinder pressure compared to the other two models. TRIF has the best agreement in terms of AHRR for the combustion of the main injection.

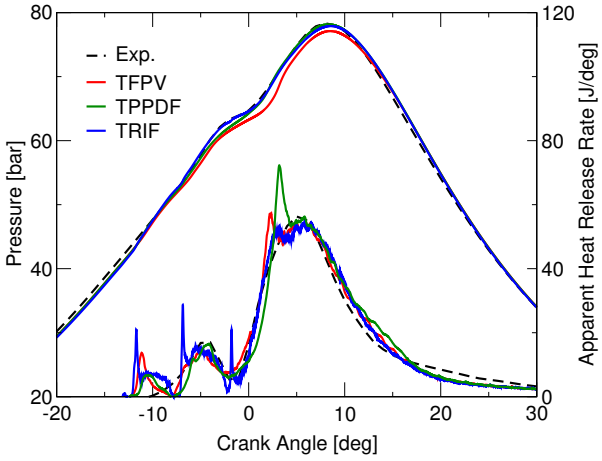

Figure 17: Comparison between computed and experimental data of in-cylinder pressure and apparent heat release rate for the operating point A25.

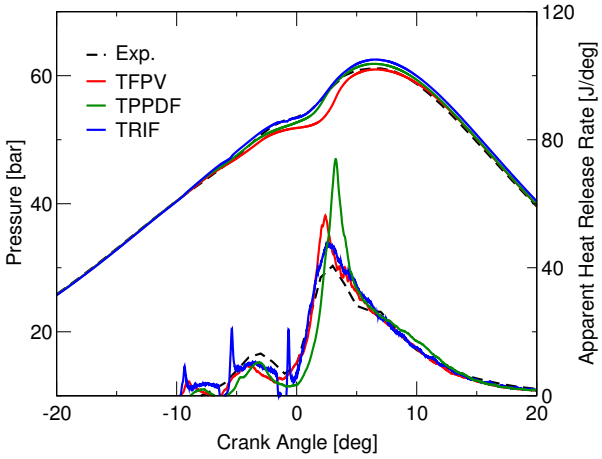

Figure 18: Comparison between computed and experimental data of in-cylinder pressure and apparent heat release rate for the operating point HEGR.

To complete the analysis on the combustion process, Figs. 19 and 20 provide an overview of the model capability to predict combustion phasing on all the tested operating points. In particular, in Fig. 19 for any combustion model the x-axis reports the experimental value of maximum cylinder pressure and the y-axis the computed one. In the case of perfect matching, points would lie on the dashed black line. For all the tested operating conditions, the maximum error in terms of predicted cylinder pressure is less than 3% which can be considered rather satisfactory. In terms of peak-pressure location, Fig. 20 illustrates that all the models predicts it with a maximum error of 1 CAD which is acceptable.

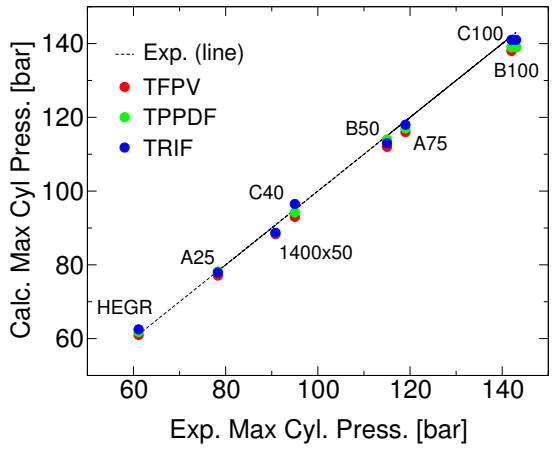

Figure 19: Experimental vs predicted maximum cylinder pressure by the TFPV, TPDF and TRIF models for any tested operating condition.

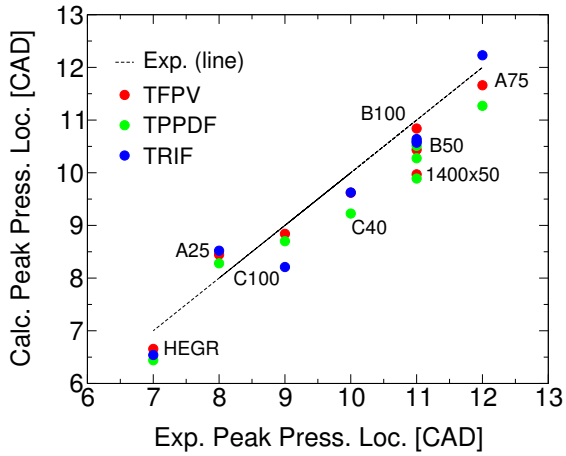

Figure 20: Experimental vs predicted maximum cylinder pressure location by the TFPV, TPDF and TRIF models for any tested operating condition.

Concerning the NO_x emissions, Fig. 21 reports the evolution of in-cylinder average NO_x concentration during the combustion and expansion phases of the four points which were used for the combustion process analysis (C100, B50, A25, HEGR). Data were normalized with respect to the maximum value of the experimental NO_x emissions. Results of the NO_x model are available only with TFPV and TPPDF, since it is not incorporated in the TRIF solver. Evolution of NO_x follows the expected trends: it grows during the combustion process and stabilizes at its maximum value when in-cylinder temperatures become low enough to promote any further nitrogen oxide formation. Since the NO_x model does not account for turbulence-chemistry interaction and sub-grid mixing and in-cylinder thermodynamic conditions are rather similar for TFPV and TPPDF, it is correct that these two models produce very similar results. Results are slightly overpredicted for the C100 condition at the highest load, while a rather good agreement was found for the other load points with lower speed.

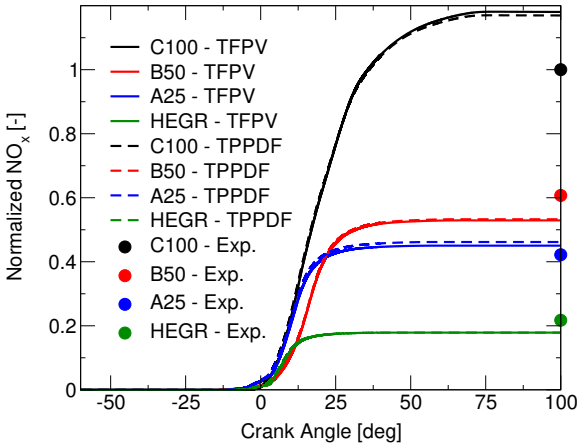

Figure 21: Computed evolution of in-cylinder average normalized NO_x concentration during the combustion and expansion process.

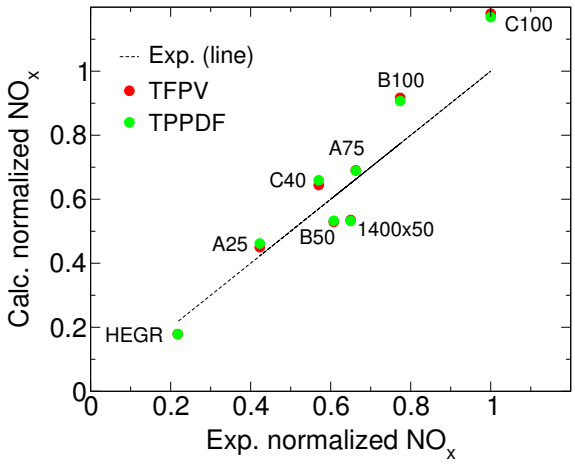

Figure 22: Experimental vs predicted wet NO_x emissions for the TFPV and TPPDF models for any tested operating condition.

Results in terms of NO_x emissions are summarized for all the tested operating conditions in Fig. 22: an overall satisfactory agreement was achieved, with a percentage error with respect to experimental data falling the $\pm 20\%$ range. Incorporation of turbulence/chemistry interaction in the NO_x model will be probably matter of a future work to see if this can further improve the agreement with experimental data.

Under conventional Diesel combustion conditions, the performances of the proposed combustion models can be considered generally satisfactory in terms of both combustion process and formation of NO_x. However, for a full validation, the model capabilities to predict the combustion process under advanced modes was also considered. A modified version of the F1C engine was considered, with a reduced compression ratio (~ 14) and a slightly different design of the piston bowl (see Fig. 23). Two operating points at constant speed and different loads were simulated whose details are listed in Tab. 5.

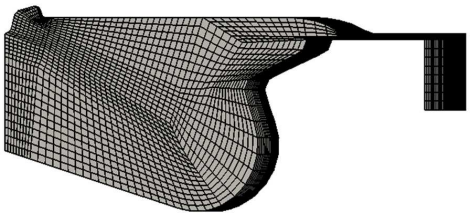

Figure 23: Computational mesh of PCCI piston bowl.

Table 5: Simulated operating points for the F1C engine under PCCI combustion mode.

	Name	speed [rpm]	bmep [bar]	λ	EGR
1	PCCI1	2000	5	1.2	40%
2	PCCI2	2000	7.5	1.2	40%

Fuel is delivered by a single injection with the SOI at approximately 25 CAD BTDC. The TWM model was used in PCCI combustion, since it is expected that effects of turbulence-chemistry interaction under such operating mode can be at first approximation neglected [33, 34]. However, in order to better capture the combined pressure/temperature effects on the ignition process, a higher temperature and pressure discretization for the chemistry table was used, whose details are reported in Tab. 6. In this case, no results sensitivity analysis to table discretization was performed and this aspect will be matter of investigation in a future work. Two different fuels were considered in the investigation: n-dodecane and the IDEA surrogate, whose chemical and physical properties are more similar to the commercial Diesel fuel [35]. IDEA is a mixture of 70% n-decane and 30% methylnaphthalene and the reduced chemical mechanism employed for table generation considers 127 species and more than 1000 reactions. Validation of such mechanism and details about the reduction algorithm can be found in [36, 37]. Four hours are necessary to generate the chemistry table for the PCCI combustion simulation.

Table 6: Temperature and pressure discretization used for the chemistry table employed in the simulation of the PCCI combustion process in the FPT F1C engine

Temperature [K]	600-800 (step 25 K)
	800 - 1000 (step 12.5 K)
	1000 - 1100 (step 25 K)
	1100 - 1200 (step 50 K)
Pressure [bar]	20-200 (step 20 bar)

Results for the PCCI1 combustion condition are reported in Figs. 24-25 in terms of cylinder pressure (a) and AHRR (b), respectively. As expected, experiments report a very fast combustion process with a high premixed peak. Moreover, a cool flame is clearly present in both the tested conditions. In the simulations, the effect of the kinetic mechanism is quite important: n-dodecane combustion is characterized by a very short cool flame period and generally underpredicts the experimental ignition delay. When us-

ing the IDEA fuel, cool flame ignition delay is rather well predicted but heat release rate during the main combustion process is slower than in the experimental data. Results can be considered acceptable in both the cases since qualitative aspects of PCCI combustion are reproduced in terms of heat release rate profile and also in both the cases maximum cylinder pressure values similar to experimental data are achieved. IDEA better estimates the ignition delay, while predicted combustion duration when using n-dodecane is in better agreement with experimental data.

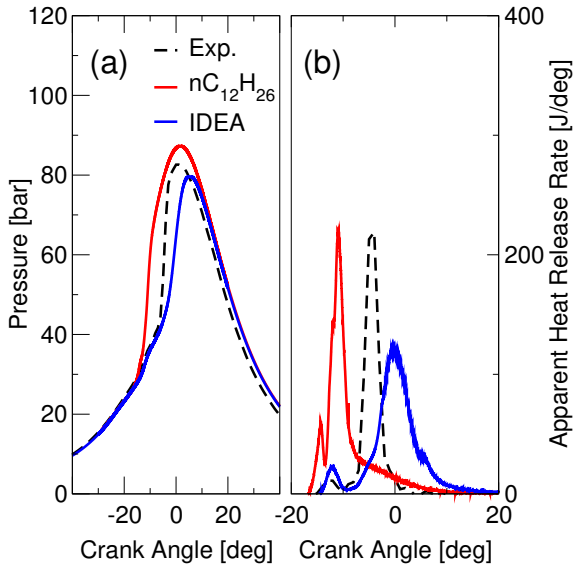

Figure 24: Comparison between computed and experimental data of in-cylinder pressure (a) and apparent heat release rate (b) for the operating point PCCI1.

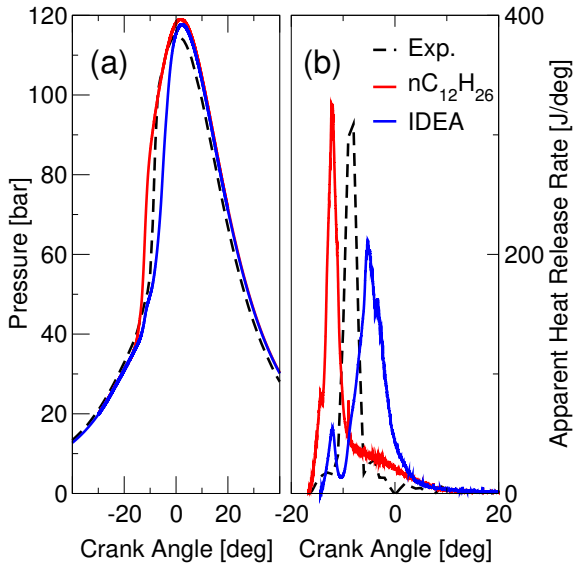

Figure 25: Comparison between computed and experimental data of in-cylinder pressure (a) and apparent heat release rate (b) for the operating point PCCI2.

Despite all the uncertainties related to spray modeling, grid dependency and validity of the tested kinetic mechanisms, further investigations are necessary to fully assess the proposed approach under advanced combustion modes, to better clarify:

- The influence of sub-grid mixing and for this reason simulations with the TFPV and TRIF model will be carried out;
- The effects of mixing-chemistry interaction: the possibility to generate TFPV tables using detailed chemistry and not tabulated reaction rates will be explored since it will make in principle possible to remove the progress variable limitation for rich equivalence ratio and this is expected to better reproduce the ignition process under a wide range of mixture fraction conditions.

Conclusions

This work was focused on the simulation of Diesel combustion using tabulated kinetics. The chemistry table is based on homogeneous constant pressure reactor calculations and tabulated reaction rate values were used as source terms in progress variable transport equation by the proposed approaches which are based on four different flame structures: well-mixed (TWM), presumed PDF (TPPDF), representative interactive flamelets (TRIF) and flamelet progress variable (TFPV) with this last model specifically developed within this work. Tabulated chemistry was also employed for the estimation of NO_x emissions. Under constant-volume combustion conditions and considering variations of ambient temperature and oxygen concentration, the TFPV model agrees rather well with experimental data of ignition delay, flame lift-off and heat release rate. Models including turbulence-chemistry interaction (TRIF, TPPDF and TFPV) have the best agreement with engine experimental data under conventional Diesel combustion where most of the heat is released under the mixing controlled-mode and ignition delay is small. In the different tested conditions, including multiple injections, different EGR rates, speeds and loads, TFPV has the better capability to predict combustion in presence of multiple injections, since it accounts for both sub-grid mixing and diffusion of progress variable in the computational domain. However, the computational time required to generate the TFPV table is significantly higher than the time needed for the other ones but it could be acceptable for the optimisation of the combustion chamber geometry since IVC conditions remain identical. In terms of NO_x, TFPV and TPPDF models provide acceptable predictions. Incorporation of tabulated NO_x in TRIF will probably make possible to have a very fast solution in terms of required time for chemistry table generation and proper estimation of combustion process and NO_x and for this reason authors will surely consider this approach in future works. Simulation of advanced combustion modes require probably a

better description of the mixing-chemistry interaction to properly predict auto-ignition: under such conditions, approaches based on progress variable reaction rate based on constant-pressure homogeneous reaction calculation show their limitations. For this reason, detailed chemistry will be directly employed in future works for the generation of the TFPV tables and also other tabulated approaches, like reaction diffusion manifolds (REDIM) will be also evaluated together with different kinetic schemes to better describe the oxidation process of the real fuels employed in IC engines.

Contact Information

Prof. Tommaso Lucchini
Department of Energy, Politecnico di Milano
Via Lambruschini, 4
20156 Milano, Italy
tommaso.lucchini@polimi.it

References

1. V. Betageri and R. Mahesh. Effects of the Real Driving Conditions on the NOx Emission of a Medium Duty Diesel Commercial Vehicle. *SAE Paper*, 2017-26-0124, 2017.

2. W. Moore, T. Finch, and M. Sutton. Development of Heavy Duty Diesel Real World Drive Cycles for Fuel Economy Measurements. *SAE Paper*, 2013-01-2568, 2013.

3. G. D'Errico, T. Lucchini, F. Contino, M. Jangi, and X.-S. Bai. Comparison of well-mixed and multiple representative interactive flamelet approaches for diesel spray combustion modelling. *Combustion Theory and Modelling*, 18(1):65–88, 2014.

4. Y. Pei, E. R. Hawkes, and S. Kook. Transported probability density function modelling of the vapour phase of an n-heptane jet at diesel engine conditions. *Proceedings of the Combustion Institute*, 34(2):3039 – 3047, 2013.

5. H. Barths, C. Hasse, and N. Peters. Computational fluid dynamics modelling of non-premixed combustion in direct injection diesel engines. *International Journal of Engine Research*, 1 (3):pp. 249–267, 2000.

6. Y. M. Wright, K. Boulouchos, G. De Paola, and E. Mastorakos. Multi-dimensional Conditional Moment Closure Modelling Applied to a Heavy-duty Common-rail Diesel Engine. *SAE Paper*, 2009-01-0717, 2009.

7. C. Bekdemir, L.M.T. Somers, and L.P.H. de Goey. Modeling diesel engine combustion using pressure dependent flamelet generated manifolds. *Proceedings of the Combustion Institute*, 33(2):2887 – 2894, 2011.

8. V. Mittal, D. J. Cook, and D. Pitsch. An extended multi-regime flamelet model for {IC} engines. *Combustion and Flame*, 159(8):2767 – 2776, 2012.

9. C. Pera, O. Colin, and S. Jay. Development of a fpi detailed chemistry tabulation methodology for internal combustion engines [dveloppement d'une tabulation fpi pour la prise en compte de la chimie complexe dans la simulation 3d moteurs]. *Oil and Gas Science and Technology*, 64(3), 2009.

10. B. Naud, R. Novella, J.M. Pastor, and J.F. Winklinger. Rans modelling of a lifted h2/n2 flame using an unsteady flamelet progress variable approach with presumed pdf. *Combustion and Flame*, 162(4):893–906, 2015.

11. J-B. Michel, O. Colin, C. Angelberger, and D. Veynante. Using the tabulated diffusion flamelet model adf-pcm to simulate a lifted methaneair jet flame. *Combustion and Flame*, 156(7):1318 – 1331, 2009.

12. T. Lucchini, Gianluca D'Errico, Angelo Onorati, Alessio Frassoldati, and Alessandro Stagni annd Gilles Hardy. Modeling non-premixed combustion using tabulated kinetics and different flame structure assumptions. *SAE International Journal of Engines*, 2017, in press.

13. H. Lehtiniemi, Y. Zhang, R. Rawat, and F. Mauss. Efficient 3-D CFD Combustion Modeling with Transient Flamelet Models. *SAE Paper*, 2008-01-0957, 2008.

14. T. Lucchini, G. D'Errico, A. Onorati, G. Bonandrini, L. Venturoli, and R. Di Gioia. Development and Application of a Computational Fluid Dynamics Methodology to Predict Fuel-Air Mixing and Sources of Soot Formation in Gasoline Direct Injection Engines. *International Journal of Engine Research*, 15 (5):pp. 581–596, 2014.

15. M.J. Wankhede, F.A. Tap, P. Schapotschnikow, and W.J.S. Ramaekers. Numerical study of unsteady flowfield and flame dynamics in a gas turbine model combustor. *Proceedings of the ASME Turbo Expo*, 4A, 2014.

16. R. Aglave, U. Riedel, and J. Warnatz. Turbulence-Chemistry Interactions in CFD Modelling of Diesel Engines. *Combustion Theory and Modelling*, 12(2):pp. 305–328, 2008.

17. A. Krisman, J.C.K. Tang, E. R. Hawkes, D. O. Lignell, and J. H. Chen. A {DNS} evaluation of mixing models for transported {PDF} modelling of turbulent nonpremixed flames. *Combustion and Flame*, 161(8):2085 – 2106, 2014.

18. H. Pitsch, H. Barths, and N. Peters. Three Dimensional Modeling of NOx and Soot Formation in DI-Diesel Engines Using Detailed Chemistry Based on the Interactive Flamelet Approach. *SAE Paper 962057, SAE Transactions*, 105(4):2010–2025, 1996.

19. T. Lucchini, M. Fiocco, A. Onorati, A. Montanaro, L. Allocca, P. Sementa, B. M. Vaglieco, and F. Catapano. Full-cycle cfd modeling of air/fuel mixing process in an optically accessible gdi engine. *SAE International Journal of Engines*, 6(3):1610–1625, 2013.

20. G. D'Errico, T. Lucchini, G. Hardy, F. Tap, and G. Ramaekers. Combustion Modeling in Heavy Duty Diesel Engines Using Detailed Chemistry and Turbulence-Chemistry Interaction. *SAE Paper*, 2015-01-0375, 2015.

21. F. V. Bracco. Modeling of Engine Sprays. *SAE Paper*, 850394, 1985.

22. R. D. Reitz. Modeling Atomization Processes In High Pressure Vaporizing Sprays. *Atomization and Spray Technology*, Vol. 3:pp. 309–337, 1987.

23. Baumgarten C. *Mixture formation in internal combustion engines*. Springer, 2006.

24. G. D'Errico, T. Lucchini, A. Onorati, and G.Hardy. Computational fluid dynamics modeling of combustion in heavy-duty diesel engines. *International Journal of Engine Research*, 16 (1):pp. 112–124, 2015.

25. T. Lucchini, G. D'Errico, H. Jasak, and Z. Tukovic. Automatic Mesh Motion with Topological Changes for Engine Simulation. *SAE Paper*, 2007-01-0170, 2007.

26. T. Lucchini, G. D'Errico, F. Brusiani, and G. Bianchi. A Finite-Element Based Mesh Motion Technique for Internal Combustion Engine Simulations. *COMODIA 2008*, MS2-3, 2008.

27. A. Frassoldati, G. D'Errico, T. Lucchini, A. Stagni, A. Cuoci, T. Faravelli, A. Onorati, and E. Ranzi. Reduced kinetic mechanisms of diesel fuel surrogate for engine {CFD} simulations. *Combustion and Flame*, 162(10):3991 – 4007, 2015.

28. J. Manin, L. Pickett, and S. Skeen. Two-Color Diffused Back-Illumination Imaging as a Diagnostic for Time-Resolved Soot Measurements in Reacting Sprays. *SAE International Journal of Engines*, 6(1):1908–1921, 2013.

29. L. M. Pickett, C. L. Genzale, G. Bruneaux, L.-M L.-M. Malbec, L. Hermant, C. Christiansen, and J. Schramm. Comparison of diesel spray combustion in different high-temperature, high-pressure facilities. *SAE International Journal of Engines*, 3(2):156–181, 2010.

30. L. M. Pickett, S. Kook, and T. Williams. Visualization of diesel spray penetration, cool-flame, ignition, high-temperature combustion, and soot formation using high-speed imaging. *SAE International Journal of Engines*, 2(1):439–459, 2009.

31. E. Mastorakos, T.A. Baritaud, and T.J. Poinsot. Numerical simulations of autoignition in turbulent mixing flows. *Combustion and Flame*, 109(1):198 – 223, 1997.

32. T. Lucchini, A. Della Torre, G. D'Errico, G. Montenegro, M. Fiocco, and A. Maghbouli. Automatic Mesh Generation for CFD Simulations of Direct-Injection Engines. *SAE Paper*, 2015-01-0376, 2015.

33. S. Kokjohn, R. Hanson, D. Splitter, and R. Reitz. Experiments and Modeling of Dual-Fuel HCCI and PCCI Combustion Using In-Cylinder Fuel Blending. *SAE International Journal of Engines*, 2(3):24–39, 2010.

34. A. Babajimopoulos, D. N. Assanis, D. L. Flowers, S. M. Aceves, and R. P. Hessel. A fully coupled computational fluid dynamics and multi-zone model with detailed chemical kinetics for the simulation of premixed charge compression ignition engines. *International Journal of Engine Research*, Vol. 6:497–512, 2005.

35. H. J. Koss, A. Wiartella, and H. Baeker. Spray Propagation, Mixture Formation, Auto-ignition and Soot Formation of Multi-Component Fuels in a Pressure Chamber. *Technical report, IDEA-EFFECT 2nd periodic report*, 1993.

36. E. Ranzi, A. Frassoldati, A. Stagni, M. Pelucchi, A. Cuoci, and T. Faravelli. Reduced kinetic schemes of complex reaction systems: Fossil and biomass-derived transportation fuels. *International Journal of Chemical Kinetics*, 46(9):512–542, 2014.

37. A. Stagni, A. Frassoldati, A. Cuoci, T. Faravelli, and E. Ranzi. Skeletal mechanism reduction through species-targeted sensitivity analysis. *Combustion and Flame*, 163:382 – 393, 2016.